

# Fluorescence Tomography with a PDE-constrained Algorithm based on the Equation of Radiative Transfer

Hyun Keol Kim<sup>1</sup>, Jong Hwan Lee<sup>1</sup>, Andreas H. Hielscher<sup>1,2</sup>

<sup>1</sup>Department of Biomedical Engineering, Columbia University, 500 West, 120<sup>th</sup> St., New York, NY 10027, USA

<sup>2</sup>Department of Radiology, Columbia University, 660 West, 168<sup>th</sup> St., New York, NY 10327, USA

Author e-mail address: hkk2107@columbia.edu

**Abstract:** We introduce the PDE-constrained fluorescence tomography algorithm that is based on a sequential quadratic programming (SQP) method. Numerical and experimental data are presented to evaluate the performance of the new algorithm. The frequency-domain equation of radiative transfer is used as a light propagation model. The results show that the PDE-constrained approach accelerates the reconstruction process up to a factor of 10 to 15 as compared to the unconstrained approach.

©2007 Optical Society of America

OCIS codes: (170.3010) Image reconstruction techniques; (260.2510) Fluorescence

## 1. Introduction

Optical fluorescence tomography that makes use of light-emitting biomarkers has emerged as a new imaging modality for imaging of target specific molecules that provide functional information about biochemical processes preceding the development of diseases [1-3]. The light distribution due to a fluorescent source inside the medium can be described by a system of the coupled excitation and emission equations. The equation of radiative transfer (ERT) can be used as a light propagation model in all types of media with a fluorescent source inside, while its diffusion approximation (DA) is of limited accuracy in small-tissue geometries or low-scattering regions [4]. However, ERT-based fluorescence reconstruction codes [5-6] takes a much longer computation time to solve one single reconstruction case, as compared to DA-based codes. Thus it is highly desirable to develop computationally efficient image reconstruction schemes that allow for using the ERT for optical fluorescence tomography. In this paper, we present the first PDE-constrained fluorescence image reconstruction algorithm based on a reduced Hessian sequential quadratic programming (rSQP) method [7], which can lead to a significant saving in the reconstruction time. We evaluate the performance of the PDE-constrained scheme using numerical and experimental results by comparing the new algorithm with an unconstrained code that makes use of the limited-memory Broyden-Fletcher-Goldfarb-Shanno (lm-BFGS) method [5-6, 8]

## 2. Method

The generation and propagation of fluorescence light in biological tissue can be accurately modeled by two coupled frequency-domain equations of radiative transfer [7,8]:

$$\left[ (\nabla \cdot \Omega) + \mu_a^x + \mu_s^x + \mu_a^{x \rightarrow m} + \frac{i\omega}{c} \right] \psi^x(\mathbf{r}, \Omega, \omega) = \int_{4\pi} p(\Omega', \Omega) \psi^x(\mathbf{r}, \Omega', \omega) d\Omega', \quad (1)$$

$$\left[ (\nabla \cdot \Omega) + \mu_a^m + \mu_s^m + \frac{i\omega}{c} \right] \psi^m(\mathbf{r}, \Omega, \omega) = \int_{4\pi} p(\Omega', \Omega) \psi^m(\mathbf{r}, \Omega', \omega) d\Omega' + \frac{1}{4\pi} \frac{\eta \mu_a^{x \rightarrow m} \phi(\mathbf{r}, \omega)}{(1 - \omega\tau(\mathbf{r}))}, \quad (2)$$

which describes the propagation of excitation (1) and emission (2) radiances respectively. Here  $\mu_a^{x \rightarrow m}$  is the absorption coefficient of a fluorescent source in tissue, in unit of  $\text{cm}^{-1}$ ;  $\eta$  denotes the quantum yield by which the fluorescent source emits light;  $\tau(\mathbf{r})$  is the local lifetime of a fluorescent source;  $\phi(\mathbf{r}, \omega)$  denotes the excitation fluence given by  $\phi(\mathbf{r}, \omega) = \int_{4\pi} \psi^x d\Omega$  in unit  $\text{Wcm}^{-2}$ . The partially reflective boundary conditions are implemented to consider the refractive index mismatch problem at air-tissue interface [9].

The optical fluorescence tomographic problem can be formulated in more general terms as follows:

$$\begin{aligned} \min f(\psi^m) &= \frac{1}{2} \sum_{s,d} |Q_d \psi_s^m - z_{s,d}|^2 \quad \text{subject to} \\ C_s^x &= A^x \psi_s^x - b_s^x = 0; s = 1, \dots, N_s, \text{ and } C_s^m = A^m \psi_s^m - b_s^m = 0; s = 1, \dots, N_s \end{aligned} \quad (3)$$

where  $f(\psi_s^m)$  is the objective function that quantifies the difference between predictions  $Q_d\psi_s^m$  and measurements  $z_{s,d}$  of emitted light made on the tissue surface;  $C^x$  and  $C^m$  are the discretized versions of the two coupled radiative transfer equations. In this study we focus on the problem of recovering  $\mu_a^{s \rightarrow m}$  only assuming a spatially homogenous  $\tau$  and  $\eta$  distribution inside the medium. By introducing a Lagrangian function, the above PDE-constrained optimization problem can be restated as

$$L(\mu; \psi^x, \psi^m; \lambda^x, \lambda^m) = \frac{1}{2} |Q\psi^m - z|^2 + \lambda^{xT} (A^x\psi^x - b^x) + \lambda^{mT} (A^m\psi^m - b^m). \quad (4)$$

The simultaneous solutions of the forward and inverse problems can then be obtained within a general framework of the reduced Hessian SQP method [10-11], which finds the minimum to a quadratic approximation of the Lagrangian function  $L$  subject to the linearized constraints by updating both forward and inverse variables at once:

$$\mu^{k+1} = \mu^k + \alpha^k \Delta \mu^k, \quad \psi^{x,k+1} = \psi^{x,k} + \alpha^k \Delta \psi^{x,k} \quad \text{and} \quad \psi^{m,k+1} = \psi^{m,k} + \alpha^k \Delta \psi^{m,k}. \quad (5)$$

A more detailed description of the rSQP algorithm used in optical tomography can be found in reference [7].

### 3. Results

We show numerical and experimental results using the rSQP method and the lm-BFGS method. For a numerical study, we consider the circular geometry with a diameter of 2 cm, which is typical for small-animal imaging. A fluorescent heterogeneity with a diameter of 0.15cm is embedded inside the circular medium. The background medium are set as  $\mu_a^s = 0.4 \text{ cm}^{-1}$  and  $\mu_s^s = 15 \text{ cm}^{-1}$ , which is same for both excitation and emission wavelengths. The fluorescence heterogeneity has the absorption coefficient of  $\mu_a^{s \rightarrow m} = 0.05 \text{ cm}^{-1}$ . The quantum yield and fluorescence lifetime are assumed spatially constant at the values of  $\tau = 4 \text{ ns}$  and  $\eta = 0.95$ , which is taken to match the corresponding properties of fluorophore (Fluorescein) used later in the experimental study. Four external sources are located on the tissue boundary close to the target fluorescent source and sixty-six detectors are equally distributed.

Simulated data are obtained with the ERT and corrupted with different noise levels. The correlation factor  $\rho(\mu^e, \mu^r)$  and the deviation factor  $\delta(\mu^e, \mu^r)$  [7] are used as the metrics to assess the image quality:  $\rho(\mu^e, \mu^r)$  indicates the degree of correlation between exact and estimated quantities while  $\delta(\mu^e, \mu^r)$  describes the discrepancy in absolute values of exact and estimated quantities. Accordingly, the closer  $\rho(\mu^e, \mu^r)$  gets to unity,

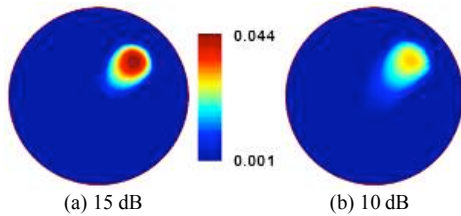


Fig. 1. Reconstructed  $\mu_a^{s \rightarrow m}$  obtained using the 15 dB and 10 dB noise data by the PDE-constrained rSQP method.

Table 1. Reconstruction quality and CPU times with different noise levels. \* denotes the acceleration factor.

SNR	Schemes	CPU time (*)	Cor. $\rho$	Dev. $\delta$
$\infty$	PDE-constr.	0.31 h (13)	0.78	<b>0.60</b>
	Unconstr.	3.98 h	0.77	0.60
15dB	PDE-constr.	0.33 h (13)	0.78	<b>0.70</b>
	Unconstr.	4.28 h	0.75	0.69
10dB	PDE-constr.	0.35 h (17)	0.66	<b>0.81</b>
	Unconstr.	5.89 h	0.64	0.78

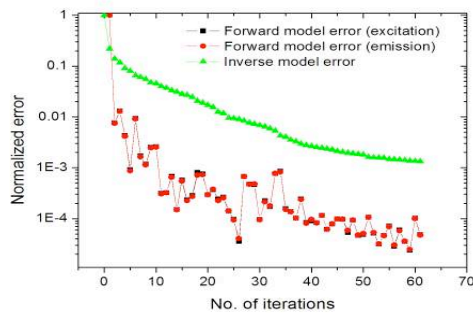


Fig. 2. Convergence history of the PDE-constrained method in the forward and inverse solutions when a loose tolerance of 0.01 is used for solving the forward problems.

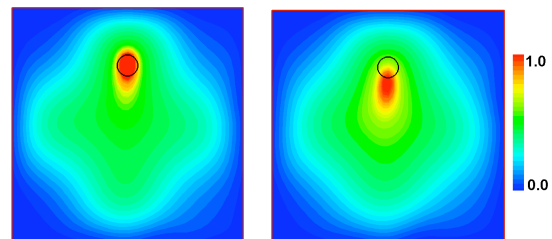


Fig. 3. Reconstructed maps of fluorophore absorption coefficients  $\mu_a^{s \rightarrow m} (\text{cm}^{-1})$  inside the phantom using the DC and 150 MHz data.

and the closer  $\delta(\mu^e, \mu^r)$  gets to zero, the better is quality of reconstruction. All the simulations are carried out on a Pentium IV 3.0 GHz CPU processor.

We compare the CPU time and the influence of noise in the PDE-constrained and unconstrained algorithms. We tested the two codes with different noise levels. Fig. 1 shows the reconstructed-  $\mu_a^{x \rightarrow m}$  maps obtained for the 15 dB case. As shown in figures, the circular fluorescence perturbation is well identified by the two methods. First the CPU times are measured for the two methods. Table 1 shows that the PDE-constrained rSQP method leads to a significant reduction in the computation time in all cases considered here. For example, with the 15dB data the PDE-constrained code takes only 0.33hrs to converge while the unconstrained code takes about 4.28hrs to meet the same convergence criterion. Therefore, the PDE-constrained method reduces the reconstruction time by a factor of about 13. The reason for this significant reduction in the CPU time is because the PDE-constrained code does not require the exact solution of the forward problem until it converges to the optimal solution, i.e., it uses the incomplete forward solution obtained with a loose tolerance, while the unconstrained code requires the complete solution of the forward problems. Fig. 2 illustrates this convergence behavior of the PDE-constrained method. It can be seen that the forward and inverse solutions converge simultaneously towards their optimal solutions, even when a loose tolerance is used. In addition to the CPU time,  $\rho(\mu^e, \mu^r)$  and  $\delta(\mu^e, \mu^r)$  are computed and the corresponding values are given in Table 1. At noise levels of 10 to 15dB, both methods make no significant difference in the accuracy.

We further studied the reconstruction of  $\mu_a^{x \rightarrow m}$  inside the medium using experimental data. The lab phantom with a square base has a size of 2.2 cm  $\times$  2.2 cm  $\times$  10.3 cm (X $\times$ Y $\times$ Z). A fluorescent cylinder rod of  $d = 2$  mm is filled with Fluorescein and embedded inside the medium. The optical properties of Fluorescein are  $\mu_a^{x \rightarrow m} = 0.4$  cm $^{-1}$ ,  $\tau = 4.0$  ns and  $\eta = 0.93$ . A cylindrical rod that contains the fluorophore is positioned about 6 mm off-center and the background medium is filled only with a 2% Intralipid solution. Each side of the phantom was illuminated by a focused light source ( $\lambda^1 = 475$  nm) and measurements of transmitted light intensities were made on the opposite side of the illumination side at  $\lambda^2 = 515$  nm, for which Fluorescein emission is largest. We obtained the measurement data for DC and 150 MHz frequency and normalized them for reconstruction. Figure 3 shows the reconstruction results. With the 150 MHz data we obtained the more accurate reconstruction in the location of the fluorescent probe as compared to the DC data, which shows that the frequency data gives better results than the DC data, especially in the identification of the target location. Note that since the source strength is not known, the reconstructed image is shown in a normalized scale [0, 1]. Again, CPU times are compared between the two methods. Here we observed a similar speedup factor as previously determined in the numerical studies. The PDE-constrained rSQP method took about 6 min. while the unconstrained lm-BFGS method required 58 min to reach the same accuracy; hence a  $\sim 10$  fold acceleration was achieved.

This work was supported in part by two grants from the National Cancer Institute (NCI-4R33CA118666 and NCI-U54CA126513-039001) at the National Institutes of Health. We also acknowledge Dr. Alexander D. Klose, Columbia University, for his many useful discussions on this study

#### 4. References

- [1] A. Garofalakis, G. Zacharakis, H. Meyer, E. N. Economou, C. Mamalaki, J. Papamatheakis, D. Kioussis, V. Ntziachristos, and J. Ripoll, "Three-dimensional in vivo imaging of green fluorescent protein-expressing T cells in mice with noncontact fluorescence molecular tomography," *Mol. Imaging* 6 (2007), 96-107.
- [2] V. Ntziachristos, R. Bremer, R. Weissleder, Fluorescence imaging with near-infrared light: new technological advances that enable in vivo molecular imaging, *Eur. Radiol.* 13 (2003) 195.
- [3] G. Choy, P. Choyke, S.K. Libutti, Current advances in molecular imaging: noninvasive in vivo bioluminescent and fluorescent optical imaging in cancer research, *Mol. Imaging* 2 (2003) 303.
- [4] A.H. Hielscher, A.E. Alcouffe, and R.L. Barbour, Comparison of finite-difference transport and diffusion calculations for photon migration in homogeneous and heterogeneous tissues, *Phys. Med. Biol.* 43, (1998) 1285-1302.
- [5] A.D. Klose, A.H. Hielscher, Fluorescence tomography with simulated data based on the equation of radiative transfer, *Opt. Lett.* 28 (2003) 1019.
- [6] A.D. Klose, V. Ntziachristos, A.H. Hielscher, The inverse source problem based on the equation of radiative transfer, *J. Comput. Phys.* 202 (2005) 323-345.
- [7] H.K. Kim, A.H. Hielscher, A PDE-constrained reduced Hessian SQP method for optical tomography based on the frequency-domain equation of radiative transfer, *Inverse Problems* 25 (2009) 015010 (20pp).
- [8] K. Ren R, G. Bal, A.H. Hielscher, Frequency domain optical tomography with the equation of radiative transfer *SIAM J. Sci. Comp.* 28 (2006) 1463-89.
- [9] M. Modest, Radiative heat transfer. New York: MacGraw-Hill Inc; 2003.
- [10] J. Nocedal and S. J. Wright, Numerical optimization, Springer-Verlag, New York, 1999.
- [11] L. Biegler, J. Nocedal, C. Schmid, D. Ternet, Numerical experience with a reduced Hessian method for large scale constrained optimization *Computational Optimization and Applications* 15 (2000) 45-67.